Low- and medium-spin negative-parity bands in the ^{187}Os nucleus

M. A. Sithole,[1,2,*] J. F. Sharpey Schafer,[3,†] E. A. Lawrie,[2,1] S. N. T. Majola,[2,3,4] A. Kardan,[5] T. D. Bucher,[1,2,6] J. J. Lawrie,[2] L. Mdletshe,[2,3] S. S. Ntshangase,[3] A. A. Netshiya,[1,2] P. Jones,[2] L. Makhathini,[2,6] K. L. Malatji,[2,6] P. L. Masiteng,[4] I. Ragnarsson,[7] B. Maqabuka,[1,2] J. Ndayishimye,[2] O. Shirinda,[2,6] B. R. Zikhali,[1,2,3] S. Jongile,[2,3,6] G. O'Neill,[1] L. Msebi,[1,2] P. M. Someketa,[8] D. Kenfack,[2,6] S. H. Mthembu,[1,2] T. C. Khumalo,[2,3] and M. V. Chisapi[2,6]

[1]*University of the Western Cape, Department of Physics, P/B X17, Bellville 7535, South Africa*
[2]*iThemba Laboratories, National Research Foundation, P.O. Box 722, Somerset West 7129, South Africa*
[3]*University of Zululand, Department of Physics, P/B X1001, KwaDlangezwa 3886, South Africa*
[4]*University of Johannesburg, Department of Physics, P.O. Box 524, Auckland Park 2006, South Africa*
[5]*School of Physics, Damghan University, P.O. Box 36716-41167, Damghan, Iran*
[6]*University of Stellenbosch, Department of Physics, P/B X1, Matieland 7602, South Africa*
[7]*Division of Mathematical Physics, LTH, Lund University, P.O. Box 118, SE-221 00 Lund, Sweden*
[8]*University of Fort Hare, Private Bag X1314, King William's Town Road, Alice 5700, South Africa*

(Received 26 August 2020; revised 20 November 2020; accepted 15 February 2021; published 26 February 2021)

Low- and medium-spin negative-parity bands of ^{187}Os have been studied using the AFRican Omnipurpose Detector for Innovative Techniques and Experiments (AFRODITE) array, following the ^{186}W(^{4}He, $3n$)^{187}Os reaction at a beam energy of 37 MeV. In the current work, all the previously known bands have been significantly extended and three new bands have been added to the level scheme. The angular distribution ratio (R_{AD}) and polarization measurements have been used to assign spin and parity to the observed new levels. The configurations of some of the bands have been modified. The observed bands are interpreted within the cranked shell model (CSM) and cranked Nilsson-Strutinsky-Bogoliubov (CNSB) formalism. Comparison with experimental data shows good agreements. Systematic comparison with the neighboring ^{185}Os isotope is also discussed.

DOI: 10.1103/PhysRevC.103.024325

I. INTRODUCTION

In a great number of odd-A transitional nuclei, structures built on neutron Nilsson orbitals associated with the $i_{13/2}$ shell have been extensively studied through in-beam γ-ray spectroscopy [1–7]. Furthermore, a number of low-lying negative-parity bands have been observed in several odd-A deformed nuclei in the 180–190 mass region [7,8]. However, despite the extensive studies, the negative-parity bands in some nuclei have not been thoroughly investigated, both experimentally and theoretically. The nucleus ^{187}Os is one of the nuclei for which there is little knowledge on the low-lying negative-parity structures. To date, known spectroscopic information about this nucleus is mainly from the electron conversion, β decay, and transfer reaction studies [9–14]. Furthermore, there is an investigation through in-beam spectroscopy [15]. In spite of this, rotational structures built on the known low-lying negative-parity levels are yet to be fully established. More importantly, accurate determinations of multipolarities of the transitions are still needed in order to confidently determine the spins and parities of the excited states, which could subsequently allow one to understand the microscopic nature of the low-spin states and parts of rotational structures reported in previous studies [7,9,11–17]. As a result, we have used the ^{186}W(α, $3n$) reaction and the AFRODITE γ-ray spectrometer to get insight into the general behavior and microscopic nature of the low-lying excitations in ^{187}Os.

II. EXPERIMENTAL DETAILS

The AFRODITE γ-ray spectrometer [18] was used to detect γ-γ coincidences produced using the ^{186}W(^{4}He, $3n$)^{187}Os reaction at 37.0 MeV. The array consisted of 11 HPGe clover detectors in BGO shields. The ^{4}He beam was delivered by the $K = 200$ separated sector cyclotron at iThemba Laboratories [19] and bombarded a stack of four ^{186}W targets, mounted on thin carbon foils with a total thickness of 400 μg/cm^2. Events of coincident γ rays were acquired if the detection of two or more γ rays occurred within a 200-ns window. A total of about 2×10^9 coincidence events were recorded and sorted into $E\gamma_1$ -$E\gamma_2$ matrices through which the level scheme for the nucleus of interest was created.

The spin-parity selection rules [20] and angular distribution ratios were used to assign multipolarity to newly observed transitions. The angular distribution ratios are given by

$$R_{AD} = \frac{I_{\gamma_1}^{135^\circ}}{I_{\gamma_1}^{90^\circ}}. \quad (1)$$

*sitholemakuhaneabel@gmail.com
†johnsharpeyschafer@gmail.com

TABLE I. The angular distribution ratios R_{AD}, the γ-ray intensities (I_γ), and the polarization asymmetries (A_P) measured for the γ-ray transitions with energies (E_γ) linking the initial and final nuclear states with energy E_i and E_f, respectively. The spin and parity assignments of these states, I_i and I_f, respectively, and the assigned multipolarity of each γ-ray (γ-Mult) are also listed. The energy of the tentative 351.5-keV transition is given in brackets. $*$ indicates the new γ rays. Empty cells refer to the information that could not be obtained. The uncertainties on the γ-ray energies are typically of 0.3 keV for strong transitions and up to 0.5 keV for weak transitions and doublets.

E_i (keV)	E_f (keV)	E_γ (keV)	I_γ	I_i^π	I_f^π	R_{AD}	A_p	γ Mult.
				Band 1				
74.4	0.0	74.4		$3/2^-$	$1/2^-$	0.46 (9)		$M1/E2$
329.9	74.4	255.5*	55.3(9)	$7/2^-$	$3/2^-$	0.86 (1)	0.22 (18)	$E2$
731.7	329.9	401.8*	36.1(12)	$11/2^-$	$7/2^-$	0.87 (1)	0.21 (11)	$E2$
1259.7	731.7	528.0*	24.8(8)	$15/2^-$	$11/2^-$	0.96 (2)		$E2$
1883.9	1259.7	624.2*	15.9(5)	$19/2^-$	$15/2^-$	0.94 (2)		$E2$
2558.6	1883.9	674.7*	8.5(3)	$23/2^-$	$19/2^-$	0.97 (2)		$E2$
3237.1	2558.6	678.5*	2.40(12)	$27/2^-$	$23/2^-$	0.94 (2)		$E2$
				Band 2				
187.2	0.0	187.2	5.9(3)	$5/2^-$	$1/2^-$	0.80 (3)		$E2$
187.2	9.8	177.4	8.9(6)	$5/2^-$	$3/2^-$	0.73 (2)		$M1/E2$
508.1	187.2	320.9	20.7(10)	$9/2^-$	$5/2^-$	0.84 (2)		$E2$
508.1	190.5	317.6*	5.3(3)	$9/2^-$	$7/2^-$	0.88 (7)		$M1/E2$
951.2	508.1	443.1*	15.1(6)	$13/2^-$	$9/2^-$	0.72 (3)		$E2$
951.2	511.3	439.9*	3.9(3)	$13/2^-$	$11/2^-$	0.47 (2)		$M1/E2$
1494.8	951.2	543.6*	9.6(4)	$17/2^-$	$13/2^-$	0.97 (3)		$E2$
2110.6	1494.8	615.8*	6.6(3)	$21/2^-$	$17/2^-$	0.93 (4)		$E2$
2762.0	2110.6	651.4*	2.15(14)	$25/2^-$	$21/2^-$	0.77 (8)		$E2$
				Band 3				
190.5	9.8	180.7	21.4(6)	$7/2^-$	$3/2^-$	0.84 (1)		$E2$
511.3	190.5	320.8	36.7(12)	$11/2^-$	$7/2^-$	0.88 (1)	0.11 (19)	$E2$
956.6	511.3	445.3*	31.1(10)	$15/2^-$	$11/2^-$	0.86 (2)	0.05 (18)	$E2$
1492.1	956.6	535.4*	5.9(6)	$19/2^-$	$15/2^-$	0.88 (4)		$E2$
1492.1	935.0	557.1*	21.1(7)	$19/2^-$	$15/2^-$	0.98 (2)		$E2$
1492.1	1209.6	282.4*	6.9(3)	$19/2^-$	$17/2^-$	0.44 (4)		$M1/E2$
2102.1	1492.1	610.0*	24.9(8)	$23/2^-$	$19/2^-$	1.03 (4)		$E2$
2729.5	2102.1	627.4*	10.7(4)	$27/2^-$	$23/2^-$	1.05 (3)		$E2$
				Band 4				
459.3	100.5	358.8	30.6(15)	$11/2^-$	$7/2^-$	0.81 (2)		$E2$
459.3	263.1	196.1	100(4)	$11/2^-$	$9/2^-$	0.56 (4)		$M1/E21$
935.0	459.3	475.7	49.0(17)	$15/2^-$	$11/2^-$	0.82 (2)		$E2$
935.0	684.4	250.3	22.5(8)	$15/2^-$	$13/2^-$	0.40 (3)		$M1/E2$
1511.6	935.0	576.6*	5.9(6)	$19/2^-$	$15/2^-$	0.96 (9)		$E2$
1511.6	956.6	554.9*	11.2(4)	$19/2^-$	$15/2^-$	0.79 (2)		$E2$
1511.6	1209.6	301.7*	8.3(4)	$19/2^-$	$17/2^-$	0.24 (11)		$M1/E2$
2145.4	1511.6	633.8*	16.3(6)	$23/2^-$	$19/2^-$	0.94 (6)		$E2$
2145.4	1813.7	331.4*	2.47(18)	$23/2^-$	$21/2^-$	0.34 (2)		$M1/E2$
2822.1	2145.4	676.7*	6.3(3)	$27/2^-$	$23/2^-$	0.89 (6)		$E2$
2822.1	2470.3	(351.5*)	1.61(17)	$27/2^-$	$25/2^-$	0.45 (9)		$M/E2$
				Band 5				
263.1	100.5	162.6	80.8(6)	$9/2^-$	$7/2^-$	0.45 (1)		$M1/E2$
684.4	263.1	421.2	35.1(13)	$13/2^-$	$9/2^-$	0.94 (2)		$E2$
684.4	459.3	225.3	37.7(13)	$13/2^-$	$11/2^-$	0.41 (2)		$M1/E2$
1209.6	684.4	525.2	32.2(11)	$17/2^-$	$13/2^-$	0.90 (1)		$E2$
1209.6	935.0	274.8	19.0(7)	$17/2^-$	$15/2^-$	0.58 (3)		$M1/E2$
1813.7	1209.6	604.1*	25.8(9)	$21/2^-$	$17/2^-$	0.93 (3)		$E2$
1813.7	1511.6	302.3*	5.9(6)	$21/2^-$	$19/2^-$	0.42 (8)		$M/E2$
2470.3	1813.7	656.6*	9.6(4)	$25/2^-$	$21/2^-$	0.94 (3)		$E2$
2470.3	2145.4	325.3*	2.89(21)	$25/2^-$	$23/2^-$			$M1/E2$
3136.0	2470.3	665.7*	3.64(20)	$29/2^-$	$25/2^-$	0.90 (3)		$E2$

TABLE I. (*Continued*).

E_i (keV)	E_f (keV)	E_γ (keV)	I_γ	I_i^π	I_f^π	R_{AD}	A_p	γ Mult.
				Band 6				
444.9	100.5	344.4	15(4)	$9/2^-$	$7/2^-$	0.37 (2)		$M1/E2$
444.9	263.1	181.9*	5.5(14)	$9/2^-$	$9/2^-$			$M1/E2$
947.7	444.9	503.0*	9.7(5)	$13/2^-$	$9/2^-$	0.82 (3)		$E2$
947.7	459.3	488.2*	10.4(6)	$13/2^-$	$11/2^-$	0.48 (4)		$M1/E2$
947.7	687.4	260.6*	4.1(3)	$13/2^-$	$11/2^-$	0.24 (10)		$M1/E2$
1532.0	947.7	584.3*	12.0(6)	$17/2^-$	$13/2^-$	0.75 (2)		$E2$
2176.7	1532.0	644.7*	4.4(3)	$21/2^-$	$17/2^-$	0.89 (8)		$E2$
				Band 7				
687.4	100.5	586.9*	6.0(6)	$11/2^-$	$7/2^-$	0.75 (2)		$E2$
687.4	263.1	424.1*	8.5(7)	$11/2^-$	$9/2^-$	0.57 (5)		$M1/E2$
687.4	444.9	242.2*	7.7(5)	$11/2^-$	$9/2^-$	0.32 (2)		$M1/E2$
1231.9	687.4	544.5*	13.4(6)	$15/2^-$	$11/2^-$	0.87 (2)		$E2$
1231.9	947.7	283.9*	6.6(4)	$15/2^-$	$13/2^-$	0.46 (2)		$M1/E2$
1231.9	684.4	547.7*	3.3(3)	$15/2^-$	$13/2^-$			$M1/E2$
1852.6	1231.9	620.7*	7.0(4)	$19/2^-$	$15/2^-$	1.07 (10)		$E2$
2512.1	1852.6	659.5*	2.23(18)	$23/2^-$	$19/2^-$	0.77 (8)		$E2$

The numerator of Eq. (1) denotes the intensity of the γ ray of interest, γ_1, detected at an angle of 135°, gated on γ_2 detected in all detectors. The denominator of Eq. (1) denotes the intensity of γ_1 detected at an angle of 90°, gated on γ_2 detected in all detectors. All the R_{AD} ratios in Table I were obtained by setting a gate on pure stretched quadrupole transitions. The measured R_{AD} ratio is close to 0.43 for a stretched dipole and close to 0.87 for a stretched quadrupole transition.

The linear polarization asymmetries A_p have been used to confirm the electromagnetic nature of the γ rays observed in this work. Here A_p is defined by

$$A_p = \frac{\alpha N_V - N_H}{\alpha N_V + N_H}, \tag{2}$$

where N_V and N_H are the number of γ rays scattered between the crystals of clover detectors at 90° perpendicular and parallel to the beam direction, respectively. The relative efficiency $\alpha = N_H/N_V$ is determined using unpolarized γ rays. For polarization measurements, the A_p values yield $A_p < 0$ and $A_p > 0$ for stretched magnetic and stretched electric transitions, respectively.

III. EXPERIMENTAL RESULTS

The nuclear structure of ^{187}Os was previously investigated by Refs. [7,9–17]. In their work, the bandheads and some low-energy levels of the rotational bands of ^{187}Os were observed. In the present study, the known structures from the previous work have been extended to higher spins. Figure 1 shows the partial decay schemes of ^{187}Os constructed using the present coincidence data. New transitions deduced in the present work are labeled in red, while transitions from previous in-beam work are labeled in black. Measured properties of γ rays and rotational levels observed in this work are listed in Table I.

Band 1 is a new rotational sequence decaying to the known 74.4-keV energy level. In the present work, six in-band transitions have been added to band 1. The angular distribution measurements carried out for all in-band transitions are consistent with stretched quadrupole ($\Delta I = 2$) nature. Figure 2 shows a spectrum with transitions associated with band 1.

Some low-spin states of bands 2–7 were observed at low spin by Ref. [15]. As shown in Fig. 1 and Table I, the present work has not only managed to confirm the existence of these bands but has also extended them to higher spins.

Band 2 has been previously observed up to $I^\pi = 9/2^-$ by Ref. [15]. In the present work, this band has been extended significantly up to $I^\pi = 25/2^-$. The R_{AD} values extracted for the in-band transitions, which include the four new transitions (443.1, 543.6, 615.8, and 651.4 keV) are consistent with stretched quadrupole ($\Delta I = 2$) nature. This band decays to band 3 through the 439.9-, 317.6-, and 177.4-keV transitions. The 177.4-keV transition was observed by the previous study [15] and its multipolarity was found consistent with mixed $M1/E2$ nature. The R_{AD} values for the 177.4- and 317.6-keV transitions measured in our work suggest that these linking transitions have either stretched quadrupole ($\Delta I = 2$) nature or mixed $M1 + E2$ nature. The R_{AD} value for the 439.9-keV transition however shows that this transition is a stretched dipole. Therefore, bands 2 and 3 have opposite signatures, in agreement with the previous spin and parity assignments for the low-energy levels of these bands. Figure 3 shows a coincidence spectrum which confirms the presence of the new transitions of band 2.

Band 3 was previously known up to $I^\pi = 11/2^-$ and only two in-band transitions, namely 180.7 and 320.8 keV, were reported by Ref. [15]. In the current work, this band has been extended up to $I^\pi = 27/2^-$ by four in-band transitions (see Figs. 1 and 4). The R_{AD} and polarization measurements deduced for the in-band transitions are consistent with them being stretched $E2$ transitions.

Bands 4 and 5 are signature partner bands built on the isomeric state at 100.5 keV with half-life of 112 ns. In the previous in-beam work [15], these bands were observed up to $I^\pi = 15/2^-$ and $I^\pi = 17/2^-$, respectively. The current study

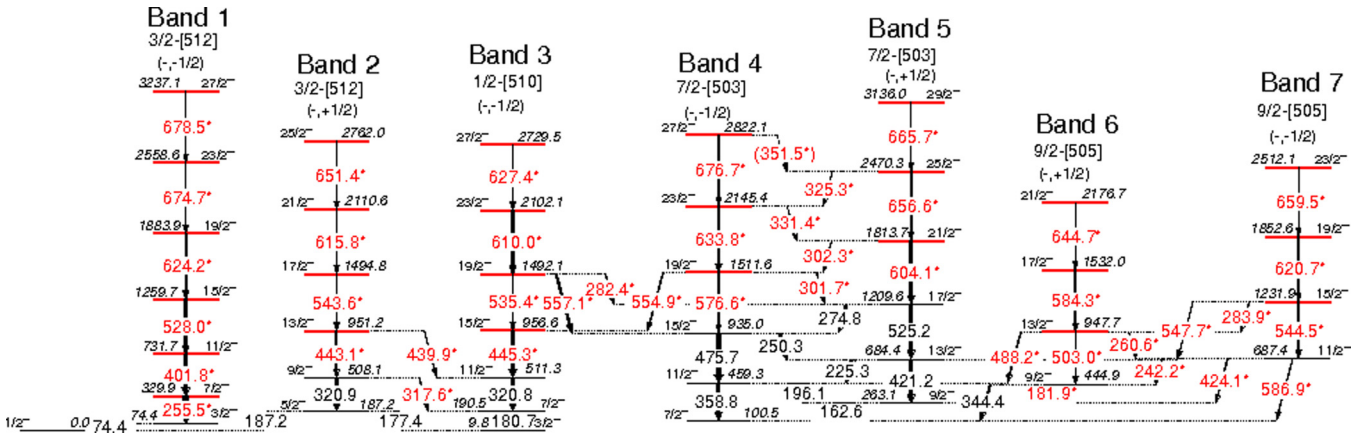

FIG. 1. Partial level scheme of ^{187}Os deduced from the current work showing the negative-parity bands. New transitions are shown in red and denoted by asterisks (*), while previously known transitions are labeled in black. Proposed configurations for each band structure are given above the bands.

does only confirm the presence of the rotational states up to the $15/2^-$ and $17/2^-$, as previously reported by Ref. [15], but has also extended these bands up to $27/2^-$ and $29/2^-$, respectively. The transitions of bands 4 and 5 are illustrated in the gated spectra shown in Figs. 5 and 6). Band 4 decays to band 5 through 196.1-, 250.3-, 301.7-, 331.4-, and 351.5-keV transitions. Two of these transitions were previously observed in Ref. [15], but their multipolarities were not measured. In the current work, the R_{AD} values for these transitions were found in agreement with stretched dipole ($\Delta I = 1$) nature. Band 5 also decays to band 4 through the 162.6-, 225.3-, 274.8-, 302.3-, and 325.3-keV transitions. The first three of these transitions are known from the previous in-beam work [15] and their multipolarities were not deduced. In the current work, the measured R_{AD} values of these transitions suggest stretched dipole ($\Delta I = 1$) nature. These measurements confirm that the two bands are signature partners. The R_{AD} and polarization asymmetry values of all the transitions in these bands are listed in Table I.

It is interesting to note that the $15/2^-$ and $19/2^-$ levels of band 4 lie at almost the same (within 22-keV) excitation energy as the corresponding levels of band 3 with the same spin and parity, and very similar excitation energies interact strongly, partly mixing their wave functions. These interactions are the cause for the observed mixing between bands 3 and 4 at these levels despite their different single-particle configurations.

Bands 6 and 7 are new bands built on the known 444.9-keV and 687.4-keV energy levels, respectively [15]. The current work has established these bands up to $I^\pi = 21/2^-$ and $I^\pi = 23/2^-$, respectively (see Fig. 1 and Table I). These bands decay to both bands 4 and 5. Band 6 decays to band 4 through the 488.2- and 344.4-keV transitions. It also decays to both bands

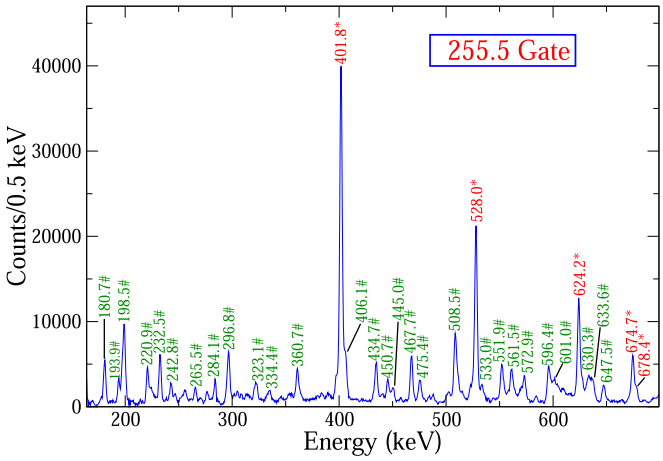

FIG. 2. Coincidence spectrum obtained by setting a gate on the 255.5-keV transition of band 1. New transitions are shown in red and denoted by asterisks (*), while contaminants and other transitions of ^{187}Os not associated with the band of interest are shown in green and labeled by hashes (#).

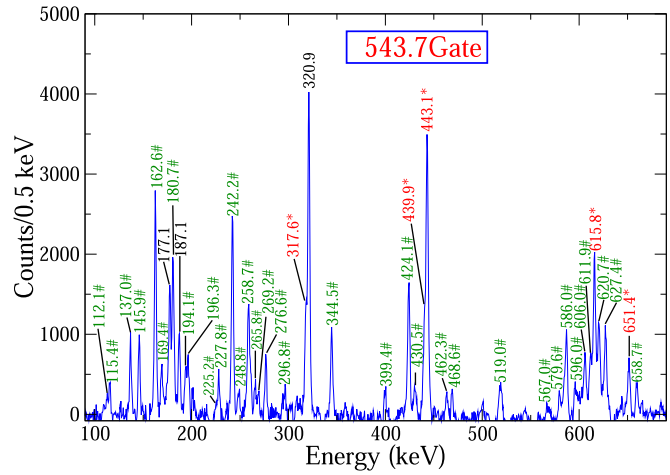

FIG. 3. Coincidence spectrum obtained by setting a gate on the 543.6-keV transition of band 2. New transitions are shown in red and denoted by asterisks (*), while contaminants and other transitions of ^{187}Os not associated with the band of interest are shown in green and labeled by hashes (#). The known transitions associated with the band of interest are shown in black.

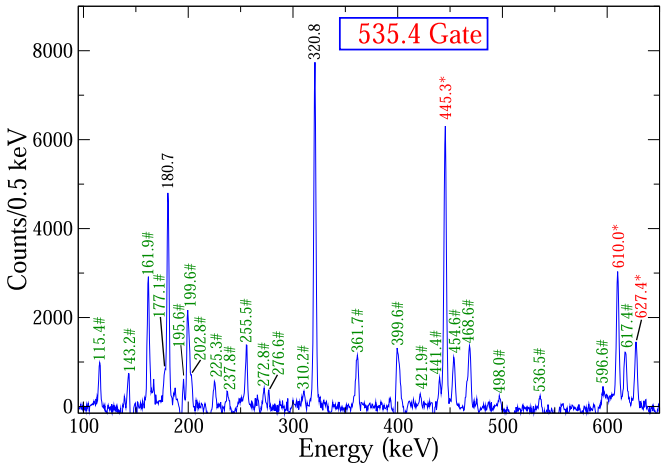

FIG. 4. Coincidence spectrum obtained by setting a gate on the 535.4-keV transition of band 3. New transitions are shown in red and denoted by asterisks (*), while contaminants and other transitions of ^{187}Os not associated with the band of interest are shown in green and labeled by hashes (#). The known transitions associated with the band of interest are shown in black.

5 and 7 through the 181.9- and 260.6-keV transitions, respectively. The $R_{\rm AD}$ values for the 488.2-, 344.4-, and 260.6-keV transitions were found to be 0.48(4), 0.37(2), and 0.24(10), respectively suggesting that these transitions have stretched dipole ($\Delta I = 1$) character. Band 7 decays to both bands 5 and 6 through the 547.7-, 424.1-, 283.9-, and 242.2-keV transitions, respectively. The $R_{\rm AD}$ values for the 424.1-, 283.9-, and 242.2-keV transitions were found to be 0.57(5), 0.46(2), and

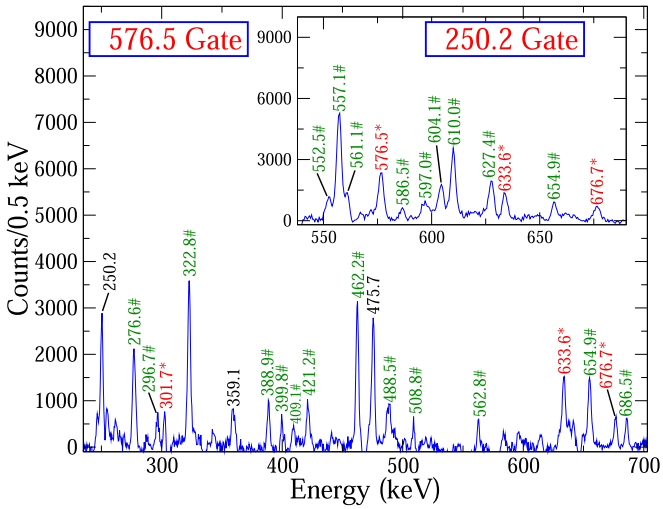

FIG. 5. Coincidence spectrum obtained by setting a gate on the 576.6-keV transition of band 4. New transitions are shown in red and denoted by asterisks (*), while contaminants and other transitions of ^{187}Os not associated with the band of interest are shown in green and labeled by hashes (#). The known transitions associated with the band of interest are shown in black. The insert shows a spectrum gated on the 250.3-keV transition to illustrate the new 576.6-keV γ ray.

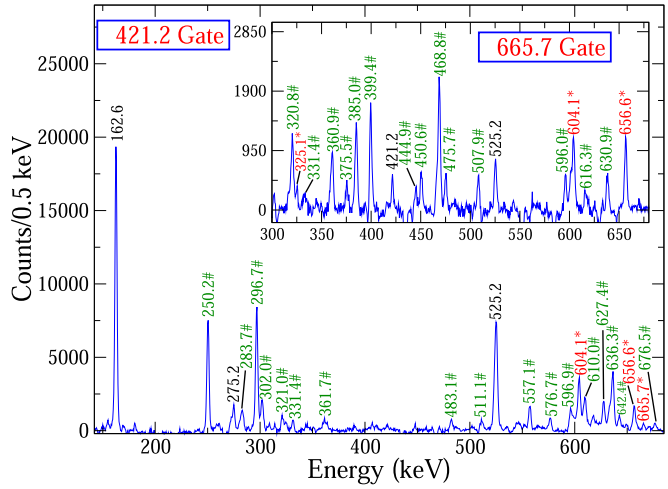

FIG. 6. Coincidence spectrum obtained by setting a gate on the 421.2-keV transition of band 5. New transitions are shown in red and denoted by asterisks (*), while contaminants and other transitions of ^{187}Os not associated with the band of interest are shown in green and labeled by hashes (#). The known transitions associated with the band of interest are shown in black. The insert shows a spectrum gated on the 665.7-keV transition to illustrate the new 604.1- and 656.6-keV γ rays.

0.32(2), respectively, suggesting stretched dipole ($\Delta I = 1$) nature. Band 7 also decays to band 4 through the 586.9-keV transition. The $R_{\rm AD}$ value of this transition is consistent with stretched quadrupole ($\Delta I = 2$) nature. The $R_{\rm AD}$ values extracted for the in-band transitions, for both bands 6 and 7 are consistent with stretched quadrupole ($\Delta I = 2$) nature. The polarization asymmetries A_p could not be obtained for the transitions in these bands because of low statistics. Figures 7

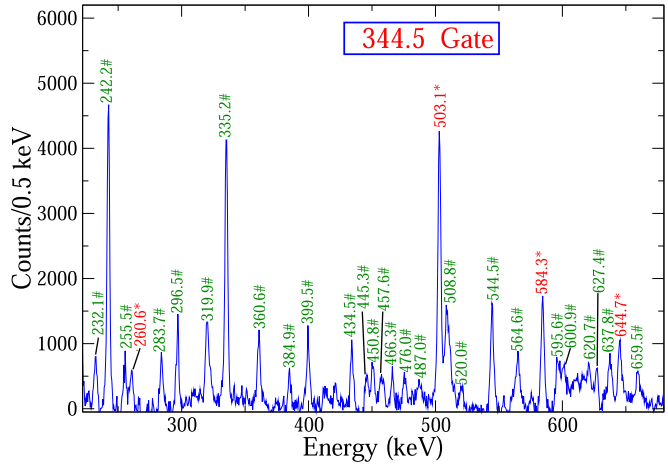

FIG. 7. Coincidence spectrum obtained by setting a gate on the 344.5-keV transition of band 6. New transitions are shown in red and denoted by asterisks (*), while contaminants and other transitions of ^{187}Os not associated with the band of interest are shown in green and labeled by hashes (#).

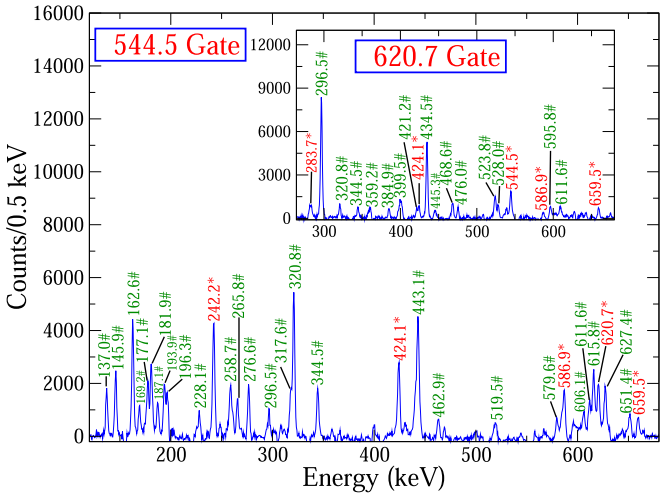

FIG. 8. Coincidence spectrum obtained by setting a gate on the 544.5-keV transition of band 7. New transitions are shown in red and denoted by asterisks (*), while contaminants and other transitions of ^{187}Os not associated with the band of interest are shown in green and labeled by hashes (#). The known transitions associated with the band of interest are shown in black. The insert shows a spectrum gated on the 620.7-keV transition to illustrate the new 544.5- and 283.9-keV γ rays.

and 8 show spectra illustrating the transitions associated with bands 6 and 7.

IV. DISCUSSION

A. Negative-parity bands in ^{185,187}Os

The excitation energy of the negative-parity bands in ^{185}Os and ^{187}Os with respect to a rigid rotor are shown in Fig. 9. The quasiparticle alignments and Routhians calculated for these bands with Harris parameter of $J_0 = 21\hbar^2$ MeV^{-1} and $J_1 = 65\hbar^4$ MeV^{-3} for ^{187}Os and $J_0 = 24\hbar^2$ MeV^{-1} and

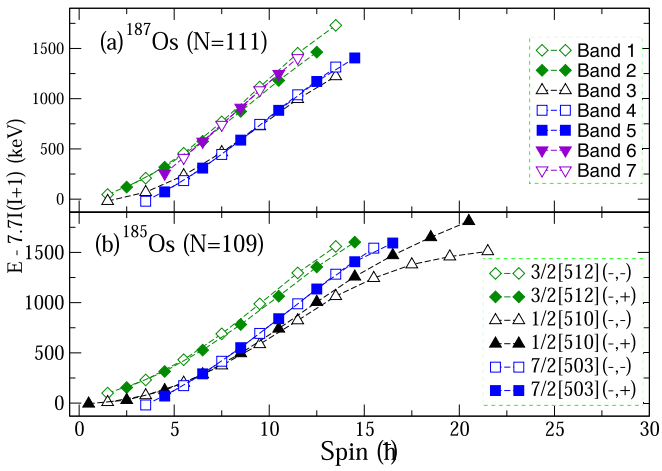

FIG. 9. The experimental excitation energies with respect to rigid rotor energies for the bands in ^{187}Os and the $3/2^-[512]$, $1/2^-[510]$, and $7/2^-[503]$ bands in ^{185}Os [21,22]. The signature partner bands are labeled in the same color, open symbols denote negative signatures, and closed symbols represent positive signatures.

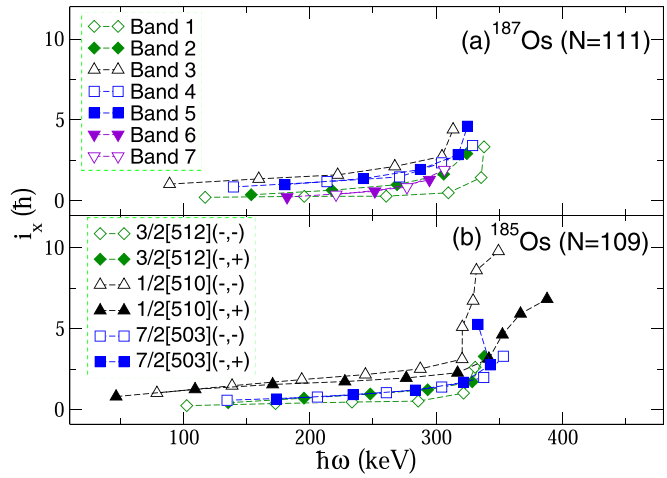

FIG. 10. Aligned angular momentum i_x deduced for the bands in ^{187}Os and ^{185}Os as a function of the rotational frequency. The Harris parameters are $J_0 = 21\hbar^2$ MeV^{-1} and $J_1 = 65\hbar^4$ MeV^{-3} for ^{187}Os and $J_0 = 24\hbar^2$ MeV^{-1} and $J_1 = 66\hbar^4$ MeV^{-3} for ^{185}Os [21].

$J_1 = 66\hbar^4$ MeV^{-3} for ^{185}Os [21] are shown in Figs. 10 and 11. In ^{187}Os, band 1 shows very similar properties to band 2 over the observed spin range and has opposite signature. This is consistent with these bands being signature partners built in the same configuration. The comparison of bands 1 and 2 of ^{187}Os with the bands assigned to the 3/2[512] configuration in ^{185}Os [see Figs. 9(b), 10(b), and 11(b)] suggests distinct similarities. For instance, the excitation energies for these bands shown in Fig. 9 show very similar trends, the measured alignment of $0.22\hbar$ for the bands in ^{187}Os is similar to the alignment of $0.23\hbar$ for the bands in ^{185}Os (see Fig. 10) and the Routhians for these bands shown in Fig. 11 look very similar as well. Therefore, bands 1 and 2 are most likely

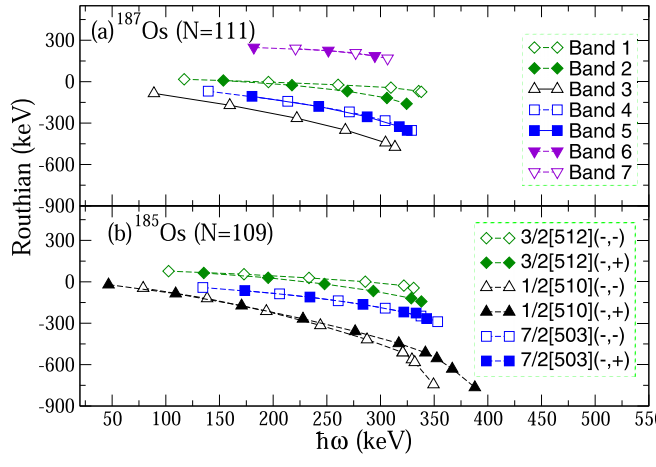

FIG. 11. The experimental Routhians for the bands in ^{187}Os and ^{185}Os. The Harris parameters for ^{187}Os are $J_0 = 21\hbar^2$ MeV^{-1} and $J_1 = 65\hbar^4$ MeV^{-3} and for ^{185}Os are $J_0 = 24\hbar^2$ MeV^{-1} and $J_1 = 66\hbar^4$ MeV^{-3} [21]. Signature partner bands are labeled in the same color, open symbols denote negative signatures, and closed symbols represent positive signatures.

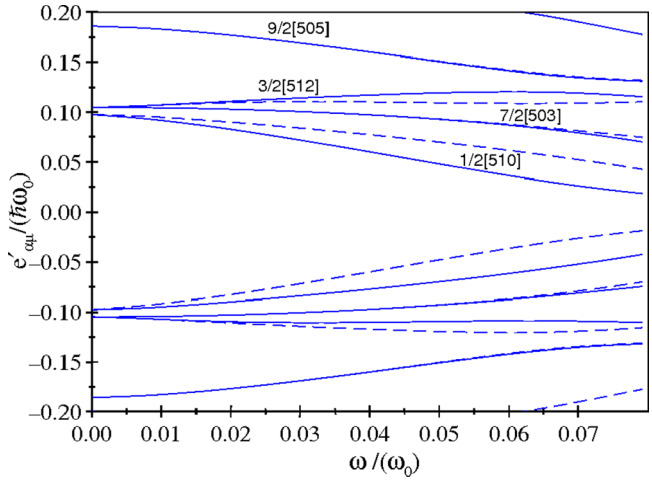

FIG. 12. Cranked shell model negative-parity Routhians for ^{186}Os with $N = 110$ as a function of the rotational frequency ω. The rotational frequency and the quasiparticle energy are expressed in units of the harmonic oscillator energy $\hbar\omega_0$. In this figure, solid lines represent quasiparticle trajectories with negative parity and signature $\alpha = 1/2$ and dashed lines are used for quasiparticle trajectories with negative parity and signature $\alpha = -1/2$.

associated with the negative and positive signatures of the 3/2[512] Nilsson configuration, respectively.

The excitation energy, the alignment, and the Routhian for band 3 in ^{187}Os are plotted in Figs. 9(a), 10(a), and 11(a). They look very similar to those of the $1/2[510](-,-1/2)$ band in ^{185}Os; see Figs. 9(b), 10(b), and 11(b). For instance, the excitation energy follows a similar trend for both nuclei, an alignment of about $1\hbar$ is measured for both bands (see Fig. 10), and the Routhians for these bands look similar and lie at lowest energy with respect to the other bands (see Fig. 11). It is therefore suggested that band 3 is associated with the negative signature of the 1/2[510] Nilsson configuration.

It should be noted that in the previous works band 2 was assigned to the ground-state configuration and thus to the $1/2[510](-,-1/2)$ configuration [7,9–17], while band 3 was assigned to the $3/2[512](-,-1/2)$ configuration [7,11–15]. It is likely that the previous works could not evaluate the behaviour of the bands at medium spins because of the limited experimental data available. They could not distinguish between the possible $1/2[510](-,-1/2)$ and $3/2[512](-,-1/2)$ configurations for these bands. The new experimental data at higher spins presented in this work allow a comparison with the bands in the neighboring ^{185}Os isotope (see Figs. 9, 10, and 11) and suggest that bands 2 and 3 have $3/2[512](-,-1/2)$ and $1/2[510](-,-1/2)$ natures, respectively.

The low-spin states of bands 4 and 5 were first observed by Harmatz *et al.* [9], who assigned them to a $K = 1/2$ band. A modification of the configuration of these bands was done by Ewbank [10], who pointed out that the 100.5-keV level has been shown to have a half-life of 112 ns and thus it could not be the $7/2^-$ member of the $K = 1/2$ band, but is probably a $7/2^-[503]$ state. The existence of this band has been confirmed by [7,9,11–17]. The band head energies of both bands 4 and 5 at 100.5 and 263.1 keV, respectively, have also been reported from the previous in-beam work [15]. These bands were considered as signature partners associated with the $7/2^-[503]$ neutron orbital. As mentioned previously, the sequence of levels added in the present work, which allowed us to observe these bands to higher spins, shows that these bands share the same moment of inertia throughout, as a function of spin; see Fig. 9(a). This feature is also displayed in the alignment and Routhian plots shown in Figs. 10(a) and 11(a), respectively. The fact that these bands are connected by interlinking $M1$ transitions and track each other over the observed frequency range is evidence that these bands are signature partners built on the same configuration. The comparison of excitation energies, alignments, and Routhians of bands 4 and 5 with the 7/2[503] bands of ^{185}Os shows a very good agreement; see Figs. 9, 10, and 11. Therefore, bands 4

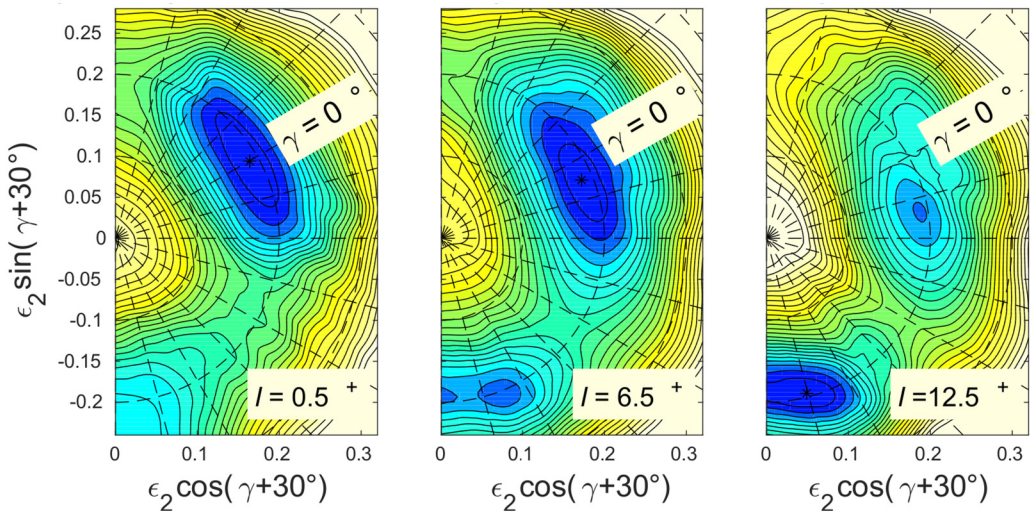

FIG. 13. Calculated total energy surfaces for the yrast $(+, 1/2)$ configuration in the CNSB formalism for increasing spin I. The contour line separation is 0.2 MeV. The absolute minima are indicated by black asterisks in each of the figures.

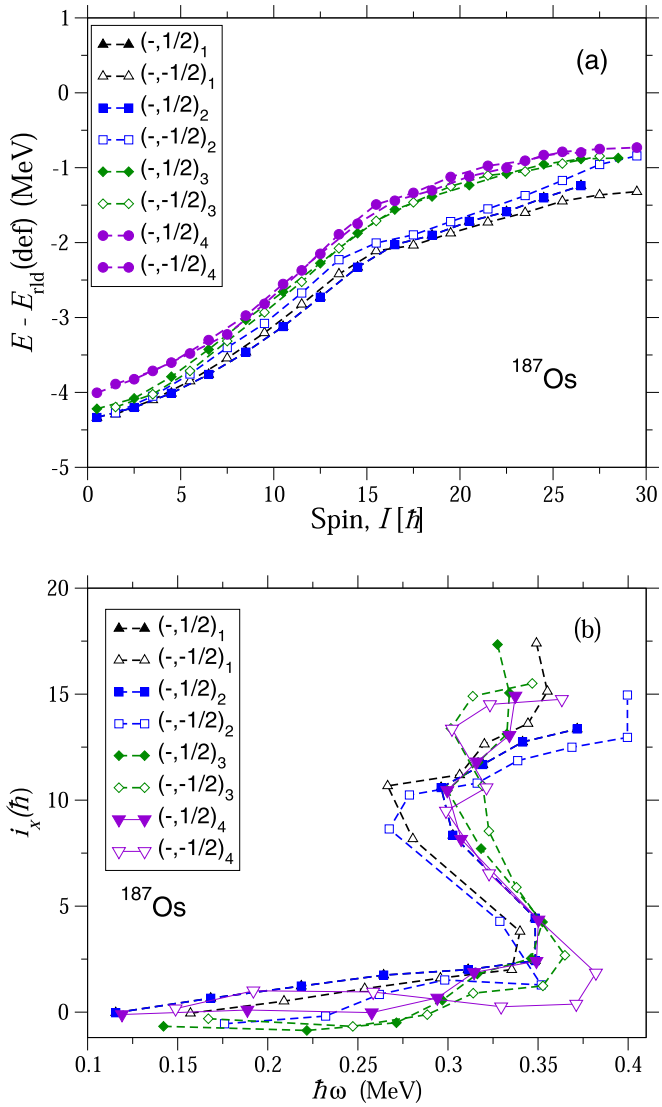

FIG. 14. (a) The excitation energies with respect to a liquid-drop reference for the four lowest energy $(-,\pm 1/2)_n$ bands of ^{187}Os calculated with the CNSB model. The index n denotes the relative energy of the bands, where $n = 1$ corresponds to the yrast negative-parity band, $n = 2$ to the first excited negative-parity band, etc. (b) The alignment of the calculated negative-parity bands in ^{187}Os as a function of rotational frequency. The Harris parameters are the same as in Fig. 10.

and 5 are assigned to the 7/2[503] Nilsson configuration. It is interesting to note that the band crossing of band 3 with bands 4 and 5 as observed in ^{187}Os was also found in ^{185}Os; see Fig. 9. This highlights further the similar behavior of these bands in the two neighboring nuclei.

The bandhead levels of bands 6 and 7 were first observed by Sodan *et al.* [15], who assigned them to a $K = 9/2$ band. The transitions that form these new bands were added in the current work and allowed us to observe these bands up to high spins. The two bands share the same moment of inertia throughout, as a function of spin; see Fig. 9(a). This feature is also displayed in the alignment and Routhian plots, shown in Figs. 10(a) and 11(a), respectively. The bands show no signature splitting [see Fig. 11(a)], which is consistent with a band associated with a neutron configuration with large Ω. Therefore, these bands are assigned as signature partners and associated with the 9/2[505] Nilsson configuration.

Further support for the proposed configurations comes from the cranked shell model (CSM) calculation shown in Fig. 12. CSM calculations were carried out with the parameters for ^{186}Os as given in Ref. [23] of $\epsilon_2 = 0.198$, $\epsilon_4 = 0.054$, $\Delta = 0.094$, $\lambda = 6.837$, $Z = 76$, and $N = 110$. The calculations suggest that the negative-parity Routhian with the lowest energy is associated with the $1/2^-[510]$ Nilsson configuration, the second lowest with the $7/2^-[503]$ configuration, the third with the $3/2^-[512]$ configuration, and the highest energy one with the $9/2^-[505]$ configuration, which is in exact agreement with the relative energy of the experimental Routhians of the bands in ^{185}Os and ^{187}Os, shown in Fig. 11. The calculations predict small signature splitting for the $7/2^-[503]$ and $3/2^-[512]$ Routhians with the negative and positive signatures being favorites for these configurations, respectively. This is also in good agreement with the experimental observations. The calculated lack of signature splitting for the $9/2^-[505]$ orbital is also in agreement with the plotted experimental Routhians of bands 6 and 7 in Fig. 11(a). The excellent agreement of the CSM calculations with the experimental data lends further support for the proposed configuration assignments.

B. Cranked Nilsson-Strutinsky-Bogoliubov formalism

Further calculations have been carried out for ^{187}Os, using the CNSB (cranked Nilsson-Strutinsky-Bogoliubov) formalism as detailed in Refs. [24–26]. Standard parameters [27] have been used in the calculations. The quantum numbers which are preserved in the CNSB approach are parity and signature; thus, for the odd-mass Os isotopes the neutron configurations are specified as (π, α). Representative CNSB potential energy surface (PES) for the yrast $(+,1/2)$ configuration is shown in Fig. 13. They identify in general the potential energy minimum as a function of the spin and of the nuclear deformation of ^{187}Os.

At the ground state, the lowest energy minimum corresponds to a well-developed prolate shape at $\varepsilon_2 \approx 0.2$. At higher spin, $I \approx 6.5$, the potential energy minimum remains at similar quadrupole deformation but shifts to a triaxial shape with $\gamma \approx -8^\circ$. At spins of $I \approx 12.5$, the nucleus becomes more triaxial and there is a competition between a rotation around its intermediate axis (the minimum at $\gamma \approx -15^\circ$) and a rotation around its long axis (the minimum at $\gamma \approx -105^\circ$), with the later minimum being the yrast one. The observed rotational bands in ^{187}Os are collective; thus, the calculations were carried out using a limitation on the deformation mesh to restrict the states to rotation around the intermediate axis (the former minimum).

The calculated single-particle energies suggest that the negative-parity low-j orbitals in the shell $N = 5$, 1/2[510], 9/2[505], 3/2[512], 7/2[503], are lying near the Fermi level for $N = 110$. Therefore, one expects that the negative-parity bands in ^{187}Os are associated with these orbitals. In the CNSB calculations the low-j orbitals are not easily distinguishable, and therefore the labeling of the negative-parity bands in

^{187}Os uses the $(-,\pm 1/2)_n$ notation, where $n = 1$ denotes the lowest-energy configuration with $(-,\pm 1/2)$, while $n = 2$ labels the second lowest-energy configuration, etc.; see, for instance, Fig. 14(a). The calculations suggest that the negative-parity bands have similar but not the same moments of inertia [see Fig. 14(a)], in agreement with the experimental data [see Fig. 9(a)]. The calculations predict very small alignments for all three negative-parity bands [see Fig. 14(b)], which is also in good agreement with the experimental data [see Fig. 10(a)]. The calculations predict an alignment of a nucleon pair at a rotational frequency of 0.30–0.35 MeV, which is also in line with the observed onset of alignment for the experimentally observed bands in Fig. 10(a). Therefore, the CNSB calculations are generally in good agreement with the proposed nucleon configurations.

V. CONCLUSION

Low- and medium-spin states in ^{187}Os were investigated using the AFRODITE array. Our work has extended all bands in ^{187}Os observed by the previous in-beam work up to high spins. Three new bands have been added in the decay scheme of ^{187}Os. The R_{AD} and polarization measurements have been used to assign spin and parity to the observed rotational bands. The negative-parity bands have been associated with the 1/2[510], 3/2[512], 7/2[503], and 9/2[505] neutron configurations. In particular, the new bands 6 and 7 are based on the 9/2[505] configuration. The negative-parity bands that have been previously assigned to 1/2[510]$(-,-1/2)$ and 3/2[512]$(-,-1/2)$ Nilsson configurations are reviewed based on the new experimental data and their configurations are swapped. Bands 4 and 5 are associated with the 7/2[503] configuration. In order to meaningfully describe the quantum behavior of the newly established structures, the cranked shell and cranked Nilsson-Strutinsky-Bogoliubov models have been used as well as a systematic comparison with the rotational bands of ^{185}Os. The good agreement between the theoretical models and the experimental data supports the proposed nucleon configurations of the negative-parity bands in ^{187}Os.

ACKNOWLEDGMENTS

It is a genuine pleasure to express our deep sense of gratitude to the iThemba Laboratory accelerator group for the beam. We thank John Simpson and the STFC Daresbury Laboratory for supplying the ^{186}W targets. Support for this work was provided by the National Research Foundation (NRF) of South Africa under Grants No. 90741, No. 95606, No. 109711, No. 96829, and No. 96829.

[1] H. X. Wang, Y. H. Zhang, X. H. Zhou, M. L. Liu, B. Ding, G. S. Li, W. Hua, H. B. Zhou, S. Guo, Y. H. Qiang, M. Oshima, M. Koizumi, Y. Toh, A. Kimura, H. Harada, K. Furutaka, F. Kitatani, S. Nakamura, Y. Hatsukawa, M. Ohta, K. Hara, T. Kin, and J. Meng, Phys. Rev. C **86**, 044305 (2012).
[2] Z. Podolyak, P. M. Walker, D. M. Cullen, G. D. Dracoulis, P. Fallon, B. Fairchild, K. Hauschild, A. O. Macchiavelli, D. P. McNabb, A. Savelius, D. Ward, and C. Wheldon, Phys. Rev. C **62**, 034303 (2000).
[3] F. K. McGowan, C. E. Bemis Jr., J. L. C. Ford Jr., W. T. Milner, D. Shapira, and P. H. Stelson, Phys. Rev. C **20**, 2093 (1979).
[4] T. Shizuma, T. Hayakawa, S. Mitarai, T. Morikawa, and T. Ishii, Phys. Rev. C **71**, 067301 (2005).
[5] T. Shizuma, T. Ishii, H. Makii, T. Hayakawa, M. Matsuda, S. Shigematsu, E. Ideguchi, Y. Zheng, M. Liu, T. Morikawa, and M. Oi, Phys. Rev. C **77**, 047303 (2008).
[6] J. Burde, M. A. Deleplanque, R. M. Diamond, A. O. Macchiavelli, F. S. Stephens, and C. W. Beausang, Phys. Rev. C **46**, 1642 (1992).
[7] A. M. Bruce, C. Thwaites, W. Gelletly, D. D. Warner, S. Albers, M. Schimmer, and P. von Brentano, Phys. Rev. C **56**, 1438 (1997).
[8] S. Jha, W. A. Seale, R. V. Ribas, E. W. Cybulska, M. N. Rao, J. D. Rogers, and G. M. Julian, Phys. Rev. C **28**, 921 (1983).
[9] B. Harmatz, T. H. Handley, and J. W. Mihelich, Phys. Rev. **128**, 1186 (1962).
[10] W. B. Eubank, Nucl. Data Nucl. Data B1 , 2-23 (1966).
[11] S. G. Malmskog, V. Berg, B. Fogelberg, and A. Bäcklin, Nucl. Phys. A **166**, 573 (1971).
[12] K. Ahlgren and P. J. Daly, Nucl. Phys. A **189**, 368 (1972).
[13] P. Morgen, B. S. Nielsen, J. Onsgaard, and C. Søndergaard, Nucl. Phys. A **204**, 81 (1973).
[14] R. Thompson and R. K. Sheline, Phys. Rev. C **7**, 1247 (1973).
[15] H. Sodan, W. D. Fromm, L. Funke, K. H. Kaun, P. Kemnitz, E. Will, G. Winter, and J. Berzins, Nucl. Phys. A **237**, 333 (1975).
[16] H. L. Sharma and N. M. Hintz, Phys. Rev. C **13**, 2288 (1976).
[17] R. Sahu, M. Satpathy, and L. Satpathy, Phys. Rev. C **23**, 1777 (1981).
[18] J. F. Sharpey-Schafer, Nucl. Phys. News Int. **14**, 5 (2004).
[19] J. L. Conradie, P. J. Celliers, J. G. de Villiers, J. L. G. Delsink, H. du Plessis, J. H. du Toit, R. E. F. Fenemore, D. T. Fourie, I. H. Kohler, C. Lussi, P. T. Mansfield, H. Mostert, G. S. Muller, G. S. Price, P. F. Rohwer *et al.*, Improvements to the iThemba LABS Cyclotron Facilities, Cyclotrons'07, Catania, October 2007.
[20] K. S. Krane, *Introductory Nuclear Physics* (John Wiley & Sons, New York, 1988).
[21] T. Shizuma, S. Mitarai, G. Sletten, R. A. Bark, N. L. Gjørup, H. J. Jensen, M. Piiparinen, J. Wrzesinski, and Y. R. Shimizu, Phys. Rev. C **69**, 024305 (2004).
[22] C. Wheldon, A. E. Stuchbery, A. N. Wilson, G. D. Dracoulis, A. M. Bruce, R. A. Bark, A. P. Byrne, F. M. Prados-Estevez, G. J. lane, C. B. Moon, J. N. Orce, and R. Wood, Eur. Phys. J. A **19**, 319 (2004).
[23] R. Bengtsson, S. Frauendorf, and F. R. May, At. Data Nucl. Data Tables **35**, 15 (1986).
[24] B. G. Carlsson, I. Ragnarsson, R. Bengtsson, E. O. Lieder, R. M. Lieder, and A. A. Pasternak, Phys. Rev. C **78**, 034316 (2008).
[25] H. L. Ma, B. G. Carlsson, I. Ragnarsson, and H. Ryde, Phys. Rev. C **90**, 014316 (2014).
[26] T. Bengtsson, Nucl. Phys. A **496**, 56 (1989).
[27] T. Bengtsson and I. Ragnarsson, Nucl. Phys. A **436**, 14 (1985).